D36

N79-24037

SKYNET SATELLITE ELECTRON PRECHARGING EXPERIMENTS*

Victor A. J. van Lint, David A. Fromme, Roger Stettner
Mission Research Corporation

ABSTRACT

Large surface areas ($\sim 1\ m^2$) of the Skynet I Qualification Model (SQM) satellite were exposed to the environments of a) a flux of monoenergetic electrons and b) pulsed high-intensity X-ray photons from an exploding-wire-radiator (EWR) source, separately and simultaneously. Experiments were performed with both the cylindrical solar-cell panels and the end thermal blanket exposed to these environments. The satellite was instrumented with fiber-optics isolated fast-response sensors capable of sensing and recording the time-varying electric fields and surface currents on the satellite. Spontaneous discharges of the two surfaces were characterized prior to measurements of the interaction of the System-Generated Electromagnetic Pulse (SGEMP) from the X-ray photon burst with the electron precharged surfaces.

Spontaneous discharges of thermal blankets and of solar cells differed in several respects. Solar-cell discharges resulted in much larger changes in average satellite potential, with a net satellite charge loss of $\sim 10^{-6}$ coulombs being measured. Thermal blanket discharges, however, were smaller in magnitude, with the net loss of charge less than 5×10^{-8} coulombs. During the solar-cell panel experiments, at a precharge potential well below the threshold for spontaneous discharge, a discharge which was apparently triggered by an X-ray photon pulse was observed. This triggered discharge was similar to spontaneous discharges recorded for solar panel illuminations.

A two-dimensional self-consistent finite difference computer code (SEMP) was used to predict the currents on the Skynet both with and without precharging of the thermal blanket. These calculations, which used an estimated thermal-blanket voltage profile, predicted a factor of 2 increase in satellite exterior axial currents. Measured precharged enhancement factors for peak current density varied between a factor of 2 and 5 in good agreement with the predictions. The enhancement is probably due to the effect of the tangential electric fields rather than the normal field on the photo-electron orbits. A late-time current (> 100 nsec) was observed in the measurements but not in the predictions. This current may be due to secondary electrons repelled by the surface potential.

*Work supported by Defense Nuclear Agency under Contract DNA001-77-C-0009.

INTRODUCTION

Electron charging and spontaneous discharge characterizations have been performed on a variety of materials in the form of small samples (area $\leq 10^3$ cm^2) (References 1-7). The potential profiles on insulators, as a function of electron energy, current density and time have been measured. The frequency of discharge and some characteristics of the discharge process (replacement current -- etc.) have been determined. The importance of geometric effects near the insulator-metal interface has been established. The present experiments were designed to measure the effect of precharging on the SGEMP (System-Generated Electromagnetic Pulse) response produced by an exploding-wire radiator on a large scale sample of typical satellite configuration. As a necessary prerequisite some spontaneous discharge measurements were performed.

EXPERIMENTAL DETAILS

The Skynet Qualification Model (SQM) was provided by Ford Aerospace and Communications Corporation in conjunction with a series of SGEMP investigations and was chosen as the test object. The exterior geometry of the Skynet satellite is illustrated in Figure 1. In orbit it spins around its axis, exposing to the sun the solar cell panels around the periphery. The 2 x 2 cm silicon solar cells are covered with .014 cm thick x 2 x 2 cm cover glasses. They are mounted on eight honeycomb panels comprising two fiberglass sheets around an aluminum core. The solar cells are interconnected and are electrically connected to the satellite's metal structure by the primary power wiring only. The honeycomb cores are individually electrically insulated. The top and bottom surfaces of the thermal blanket are covered with a .01 cm layer of thermal paint (white on the top shield and black on the bottom). The thermal blanket is composed of a fiberglass layer .01 cm thick over several layers of aluminized mylar .007 cm thick supported by a 1.2 cm nylon fiber honeycomb sandwiched between two .005 cm aluminum plates. The aluminum sheets are electrically connected to the satellite's metal structure. On top of the satellite a small microwave reflector is mounted on a despun motor assembly. On the spinning section this is surrounded by a grounded metal ring. In the SQM the despun assembly was replaced by a metal plate during these experiments.

Results from sensors on the inside of the SQM and from internal wiring have been reported previously (Reference 8).

The SQM was placed inside a 4 m diameter x 6 m long vacuum chamber (furnished by Air Force Weapons Laboratory) attached to the OWL II EWR source (furnished by Physics International Company) as illustrated in Figure 2. A diffuse electron gun was mounted on the front face of the chamber, exposing the surface at an angle of $\sim 30^\circ$ with respect to the EWR source. The accelerating voltage in the gun was varied between 3 and 15 keV. The current density at the sample could be adjusted up to 100 μA/m^2. The geometry and properties of the electron gun produced a nonuniformity in the current density at the irradiated surface of approximately a factor of two. The vacuum chamber was provided with a LN_2-cooled

annular cold plate surrounding the aperture in the front, which maintained the vacuum near 1×10^{-5} Torr. The chamber was provided with an electromagnetic damper in the form of two cylindrical 200-Ohm sheets at .8 and .94 tank radii and a single sheet near the back wall. Pulsed electrical measurements indicate that the resultant damping times of the tank electrical modes are less than 20 ns.

The satellite metallic structure was grounded to the tank structure through a 50 kΩ string of resistors. This provided less than 5 volt structure potentials during charging at currents up to 10^{-4} A/m^2.

The structure was nevertheless isolated during discharges and photon pulses, both of which have durations significantly less than the 10 μsec time constant of the satellite and resistor chain.

Measurements were performed using a series of EG&G CMLX3B (Reference 9) surface current sensors on the exterior of the satellite as noted in Figure 1. All of the data was acquired via fiber-optic data links (Reference 10), recorded on Tektronix 7912 transient digitizers, and processed on a PDP 11/40 computer.

The characteristics of the photon source output have been discussed in References 11 and 12. The peak emission currents from surfaces of the satellite was ~ 300 A/m^2.

The electrostatic voltage was measured at one location on the top thermal cover .15 m from the outer edge and in the middle of a solar cell cover .15 m from the top edge with Trek electrostatic voltage probes. These measurements were qualitative only, since the irregular surfaces precluded scanning the probe head and it was left in place during electron spraying. Therefore the voltage achieved by the nearby surface may have been affected by the presence of the probe. The measured potentials remained essentially constant after the electron beam was turned off as long as the chamber pressure was below 2×10^{-5} Torr.

The time derivative of the electric field was monitored on the front thermal blanket opposite the position of the electrostatic voltmeter. Two $\dot{B}$ loops were also mounted $\sim$.2 m in the front of the front thermal blanket.

CALCULATION METHODS

The calculations were not designed to predict the details of the SGEMP response but to indicate the magnitude of the effect of precharging and explore the mechanisms of triggered discharges.

Calculations were based on the hypothesis that the interaction between precharging and SGEMP response was solely the effect of the pre-existing electric fields on the photoelectron orbits. The objective of the calculations was to compare SGEMP skin currents and fields with and without precharge; no discharge model was included in the simulations. The simulations were performed with a particle follower Maxwell solver SGEMP code. The effect of the SGEMP exposure on the electric field distribution was calculated to evaluate the hypothesis that

a discharge can be triggered by an SGEMP-induced increase in local electric stress.

The potential was measured at only one point in the experiment so that a measured potential profile was not used in the code simulation. Instead, a physically reasonable profile was used which incorporated the one data point. Figure 3 shows the model used in the simulation. The experimentally measured point showed a voltage difference between the dielectric surface and substrate of 3 kV. The prescribed profile was taken to be 3 kV between dielectric and substrate out to 60 cm from the center line, for the last 10 centimeters the potential difference dropped linearly to zero.

The cell size in the simulation, 2.5 cm is much larger than the actual dielectric thickness (2×10^{-2} cm) but smaller than all other physical dimensions. Physically we wish the potential difference to reflect the change in the real charge density on the surface, σ_R, as photoelectrons are emitted. To accomplish this we can prescribe the dielectric constant in the simulation. The relationship between voltage V and real charge density for a thin flat dielectric of thickness d is given by $\sigma_R = \varepsilon V/d$. The code value of ε, ε_c is given by $\varepsilon_c = \varepsilon \Delta z/d$, where ε is the actual dielectric constant in the experiment (about 4), d is the actual dielectric thickness, and Δz is equal to the grid size in the code.

The simulations with precharge were made by first slowly placing charge on the grid elements in the computer code SEMP. During the photon pulse simulation particles were emitted from the dielectric surface using a typical time history chosen from several individual shot records and a peak emission current of 1.8×10^{-2} amp/cm^2. A linear times exponential energy distribution having an average energy of 1.6 keV was used together with a cosine angular distribution with respect to the normal. This distribution represents adequately the emitted spectrum and distribution caused by the exploding wire photon source. Simulations were made both with and without precharging using the same time history and spectrum.

The effect of the SGEMP exposure on the electric field distribution was also calculated to evaluate the hypothesis that a discharge can be triggered by an SGEMP-induced increase in local electric stress.

SPONTANEOUS DISCHARGE - THERMAL BLANKET

The nature of the spontaneous discharges observed visually on the thermal blanket and the solar cells were significantly different.

The thermal blanket discharges appeared as several small pin-points. The points were irregularly located, often near but not limited to the perimeter and mounting screws of the thermal blanket. Visually, many of these points would appear at approximately the same time.

The results from a $\dot{B}$ loop mounted in front of the front thermal blanket are shown in Figure 4. The trace shows fairly clear evidence of multiple exci-

tations over a time frame of ~ 600 nsec. Both the visual observations and the $\dot{B}$ traces shown were taken during a test period when the electron beam energy was near the threshold for breakdown and discharges occurred at a rate of 1-2 per minute as measured on the electrostatic voltage probe at a beam current of 9×10^{-5} A/c .

The electrostatic voltmeter trace (Figure 5) provides a record of a typical thermal blanket charging/discharging sequence. The initial charging is typical of a charging capacitor and has been studied in detail on small samples, with movable voltage probes which provide a better measure of the surface potential distribution. There are two significant features of the discharges, indicated by slight vertical deflections in Figure 5. The first is that the discharge did not occur below a certain threshold beam energy, which corresponds to a threshold potential. The second feature is that a discharge seems to represent a minor perturbation of the surface potential at the probe location. The probe is at a fixed point and the discharges could be remote (~ .5 m) from the probe. Nevertheless, the discharges do not seem to involve the entire area (or even a large fraction of the area) since the voltage does not drop significantly.

The $\dot{E}$ probe, located 180° opposite the electrostatic voltage probe, provided time resolution of the voltage change during a discharge. The traces shown in Figure 6 present the output from this probe for several of the spontaneous discharges. A feature of this $\dot{E}$ trace is the precursor (noted by the arrow in Figure 6). The precursor corresponds to an increase in the potential (less negative) over a period of ~ 200 nsec prior to the sudden onset of the main discharge lasting ~ 100 nsec.

The area of the $\dot{E}$ probe trace is approximately zero indicating the electric field (and charge) near the probe fluctuates during a thermal blanket discharge but undergoes no significant net change. This agrees with the TREK probe measurements at another location.

A second feature that should be noted is the high frequency oscillations present in the main discharge time frame. The response of the satellite structure to thermal blanket discharges was described in a previous paper (Reference 8). The satellite response when compared to previous electrical and photon tests (References 8 and 13) suggests that 1) the discharge process consists of a number of discrete fast events, 2) the discharge was far from axially symmetric, and 3) secondary excitations occur in the ~ 600 nsec time frame.

All of these results agree with the external sensor results presented in this paper.

SPONTANEOUS DISCHARGES - SOLAR CELLS

The typical solar cell discharge appeared visually as a localized line spark along the edge of one or a few solar cell cover glasses, rather than the several light spots noted on thermal blanket discharges.

Portions of the trace from the electrostatic voltmeter during a charging/discharging sequence of the solar cells is given in Figure 7. Several important features should be noted. The discharges occur above a certain threshold potential as in the thermal blanket discharges. The absolute magnitude of this threshold in these measurements is biased by the fact that the voltage probe could not move and shadows the immediate area of the measurements. The second feature (obvious in several of the discharges) is the magnitude of the voltage change. In one particular case (Figure 7b) the potential fell almost to zero volts, corresponding to a clean wipe-off of the charge on the solar cell being monitored.

The final feature (Figure 7a & 7c) is an increase in the potential of the solar cell being monitored. This occurred on several occasions and corresponds to a transfer of electrons from a surrounding solar cell to the cell being monitored.

Replacement current, measured on the 50 kΩ resistor chain (Figure 8), consistently indicated that ~ 1000 nC of electrons were transported from the model to the tank walls during solar cell discharges. This amount of charge would raise the average potential of the solar cell covers to near ground, after which electrons would no longer be accelerated to the tank walls. This amount of charge also corresponds approximately to the amount of charge stored on a single solar cell cover calculated from the measured surface potential. Figure 8b also includes an example of a second high frequency excitation ~ 600 nsec after the initial discharge.

The rise time of the replacement current is determined by the time history of the electrons leaving the model and their transit times to the tank wall. The expected electron energy at the tank wall corresponds to the average potential of the satellite. The average potential experienced by the electron will be significantly less than this due to the decrease in satellite potential (from charge emission) and to the spatial distribution of the potential. An average potential of 1 kV produces an electron transit time of several hundred nanoseconds, in reasonable agreement with Figure 8, and indicates a discharge emission time less than 100 nanoseconds. Results from sensors on the satellite presented in a previous paper (Reference 8) indicated that solar cell discharges excited external surface currents much larger than thermal blanket discharges. This agrees with the net charge loss measurements.

SGEMP RESPONSE OF PRECHARGED SATELLITE

The SQM was exposed to a series of EWR irradiations in an uncharged state and after a 10 minute exposure at 3×10^{-5} A/m^2 of electrons from the gun at 10 kV potential. The thermal cover was exposed four times (twice without charge and twice precharged). The solar cells were exposed four times (once without charge and three times precharged).

The external axial current density for thermal blanket irradiation is compared in Figure 9 with the results of the computer predictions. Both the calcu-

lations and measurements exhibit an increase in peak current compared to the uncharged response.

This peak current increase due to precharging is probably due to the modification of electron orbits by the tangential electric field. The static normal field due to charging is $\sim 10^4$ V/m and is small compared to the measured space charge fields of 10^5 V/m (Reference 14). A previous experiment and calculations with a metal disk charged to -10 kV indicated less than a 30% change in SGEMP response due to a field which is normal to the surface at all points. The differential charging of a dielectric above a grounded substrate can lead to significant potential gradients on the satellite and gives rise to transverse fields that affect every electron.

The broadening of the pulse shape noted in computer predictions cannot be confirmed by the measurement since the two photon pulses did differ in pulse shape in the 0-40 nsec range. The oscillations which produce the peak at 80 nsec in the predictions and at approximately 40 nsec and 60 nsec in the measurements are due to the interaction of the interior of the satellite with the external current through the gaps between the thermal blanket and the solar panel. The late time current (> 100 nsec) noted in the measurement is not due to this difference in pulse shape and is not present in the computer simulation. The late time current may be due to secondary electrons emitted from the surface which would normally be forced back to the surface by the space charge field. In the precharged case these electrons are repelled by the surface charge and may contribute to the net current from the top to the side of the satellite. Since the code does not produce or propagate secondary electrons they do not appear in the code.

Larger peak values and broadening of the pulse shape were typical of most of the sensors on the surface and in the interior of the satellite (Reference 8).

The external axial surface current density for a solar panel illumination with and without precharging is compared in Figure 10. The peak current density increase of a factor of 2-5 was comparable to that noted on the thermal blanket measurements.

Figure 11 represents the time histories for the axial current sensor, azimuthal current sensor and an axial surface current sensor on the inside of the solar panel during one of three solar panel precharged shots. The time of the photon excitation is noted by an arrow. An intense excitation on both of the axial current sensors occurs approximately 65 nsec after the photon pulse. The threshold for spontaneous discharges on the solar panel corresponded to a beam voltage of 14 kV during the previous electron exposures. No spontaneous discharges occurred at 10 kV, which was the beam voltage used for the charging prior to the photon irradiation. Thus it is likely that the discharge observed was triggered by the photon irradiation. The response of sensors near the illuminated solar panel was much larger than those further away as expected. The characteristics of the triggered discharge are similar to the spontaneous solar cell discharge characteristics discussed earlier as far as the instrumentation and analysis available thus far would determine.

The two-dimensional code described earlier was used to investigate possible mechanisms for triggering discharges. The simplest assumption regarding the triggering mechanism for either spontaneous or triggered discharges is to assume an electric field threshold exists above which a discharge occurs. The simulation was run for a model of the thermal blanket shown schematically in Figure 12a. A potential profile consistent with the single measured potential and graded linearly to the edge of the dielectric was assumed. The solid line in Figure 12b is a histogram of the electric fields normal to the surface at positions just above the surface resulting from this linear potential. The solid lines (0 nsec) represent the field just prior to the photon pulse. The dotted and dashed lines represent the field strengths at 15 & 30 nsec after the photon pulse. The normal fields above the surface (at 15 nsec and 30 nsec) are significantly higher than the uncharged photon response and higher than the initial field due to charging. The tangential field at Position 7 is increased also. As expected near the center of the dielectric there is very little change in the electric fields within the dielectric. Near the edge (Position 4) the field within the dielectric is increased but only slightly. The radial electric field in this simulation achieves its highest value both within and above the dielectric, prior to the photon pulse; the photons merely cause a relaxation of the radial fields at the positions investigated. The magnitude of the increases predicted by this simulation are not valid estimates due to cell size limitations.

The above simulation was run for a model of the thermal blanket. The geometry of a solar cell, which has a metal tab extending beyond the dielectric, would probably enhance the effects seen on this computer model. The simulation could not contain enough detail to treat the solar cell case.

Two major points, however, can be made from the simulation. Fields in excess of those due to the initial charging can be produced by the rearrangement of charge on a dielectric during a photon pulse, and this rearrangement of charge from the pulse lasts beyond the end of the pulse. The latter could be critical in terms of providing time for a discharge to begin. Research on vacuum dielectric breakdown has indicated that short pulse voltage thresholds are higher than the threshold for long pulses.

The triggered discharge may have very serious consequences for satellite design. The existing evidence indicates that solar-panel spontaneous discharges are limited to one or a few cover glasses. If a large number of cover glasses were charged to near their spontaneous discharge threshold, an intense photon pulse could trigger a simultaneous discharge of many of them, resulting in an electrical stress to the electronics much more severe than normally encountered.

SUMMARY

Spontaneous discharges on the large area thermal blanket material differed significantly from those on the solar panels covered with 2 x 2 cm solar cells. This is to be expected since the materials are quite different (paint and quartz) with quite different surfaces which affect the secondary electron emission.

Thermal blanket discharges: (1) appeared as multiple pin points, (2) seemed to consist of multiple high frequency discrete events, and (3) corresponded to small average satellite potential changes (small net charge loss < 50 nC). Solar panel spontaneous discharges: (1) appeared to be single line discharges near the edge of one or more solar cells, (2) corresponded to large average satellite potential changes (net charge loss ~ 1000 nC), (3) sometimes represent total discharge of at least one solar cell, and (4) seem to be limited to one or a few solar cells.

The magnitude of the modification of the SGEMP surface current response for thermal blanket illumination was in good agreement with the computer simulation. Thus the modification of the electron orbits by the transverse electric field seems to explain the enhancement of the SGEMP response to first order. A late time (> 100 nsec) current was noted experimentally but not in the code predictions. This may be due to secondary electrons not in the code.

A discharge which was very probably triggered by a photon pulse was observed on the solar cells. Its characteristics were similar to a spontaneous solar cell discharge. The possibility of triggering many solar cells simultaneously could pose a serious threat to electronics. A code simulation has indicated that an increase of surface potential gradients due to charge rearrangement during a photon pulse on a precharged surface could be the mechanism for triggering a discharge at potentials below the threshold.

Many thanks to John Rutherford and IRT Corporation, San Diego for support in designing and operating the electron gun; Harry Diamond Laboratories, Nasa Lewis Research and Spire Corporation for instrumentation support.

REFERENCES

1. USAF/NASA Spacecraft Charging Technology Conference, Colorado Springs, October 27-29, 1976.

2. Hoffmaster, D. K., and J. M. Sellen, Jr., Progress in Astron. and Aeron. 47, 185 (1975).

3. Purvis, C. K., N. J. Stevens and J. C. Oglebay, NASA Technical Memorandum, NASA TM X-73606 (1976).

4. Stevens, N. J., R. R. Lovell and V. Gore, Progress in Astron. and Aeron. 47, 263 (1975).

5. Stevens, N. J., V. W. Klinect and F. D. Berkopec; NASA Technical Memorandum, NASA TM X-73467 (1976).

6. Stevens, N. J., F. D. Berkopec and R. A. Blech, NASA Technical Memorandum, NASA TM X-73436 (1976).

7. Stevens, N. J., F. D. Berkopec, J. V. Staskus, R. A. Blech and S. J. Narcisco, NASA Technical Memorandum, NASA TM X-73603 (1976).

8. van Lint, V. A. J., D. A. Fromme, and John A. Rutherford, "Spontaneous Discharges and the Effect of Electron Charging on Skynet SGEMP Response," IEEE Trans. on Nucl. Sci., NS-25, December 1978.

9. Olsen, S. , D. Pabst, and G. D. Sauer "CML-X3A(R) B-dot Sensor," (EMP Sensor Handbook SH), 15 June 1976.

10. Blackburn, J. C. and A. Brombersky, IEEE Trans. on Nucl. Sci., NS-24, 2495 (1977).

11. Bernstein, A. J., IEEE Trans. on Nucl. Sci., NS-24, 2512 (1977).

12. Fromme, D. A., V. A. J. van Lint, R. G. Stettner and C. E. Mallon, IEEE Trans. on Nucl. Sci., NS-24, 2527 (1977).

13. Fromme, D. A., V. A. J. van Lint, R. Stettner, and B. M. Goldstein, "Exploding-Wire Photon Testing of Skynet Satellite," IEEE Trans. Nuclear Sci., NS-25, December 1978.

14. Fromme, D. A., R. G. Stettner, V. A. J. van Lint, C. L. Longmire, and R. Leadon, "SGEMP Response Investigations with Exploding-Wire Photons," IEEE Trans. Nucl. Sci., NS-24, 2371 (1977).

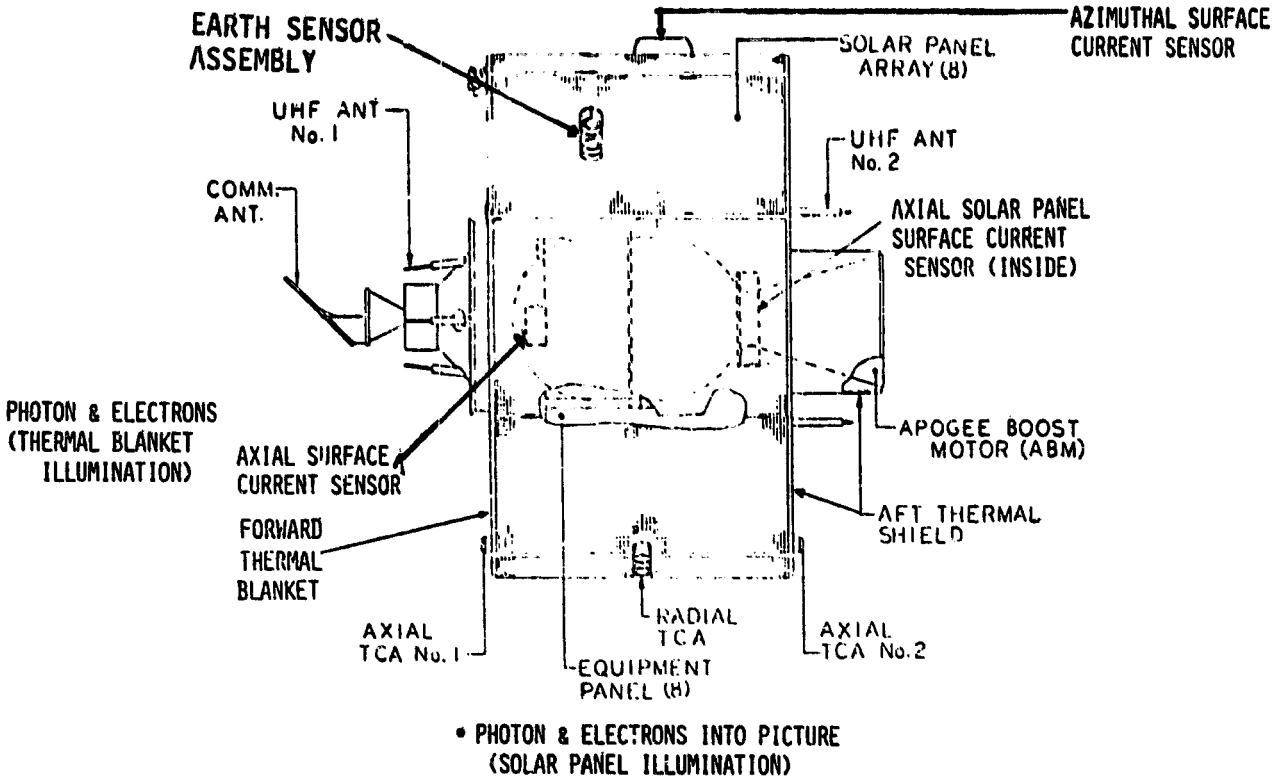

Figure 1. Skynet I satellite (side view).

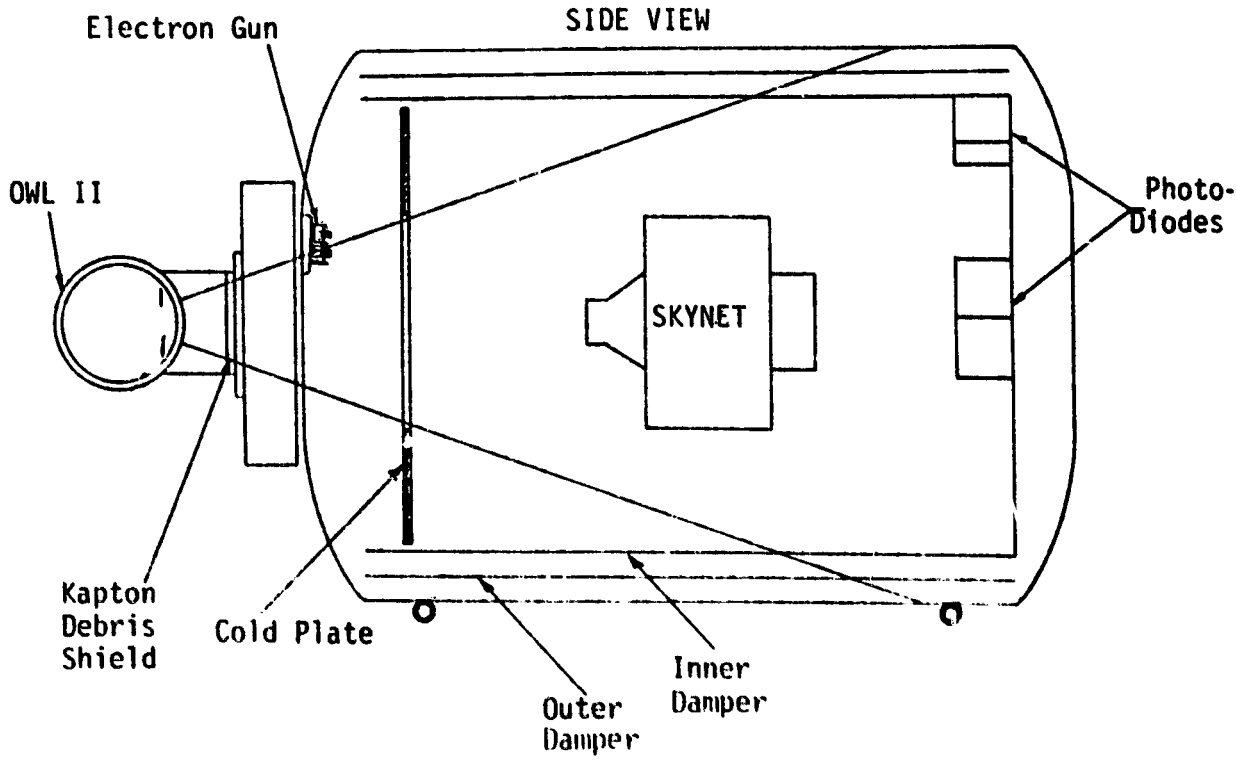

Figure 2. Skynet test setup.

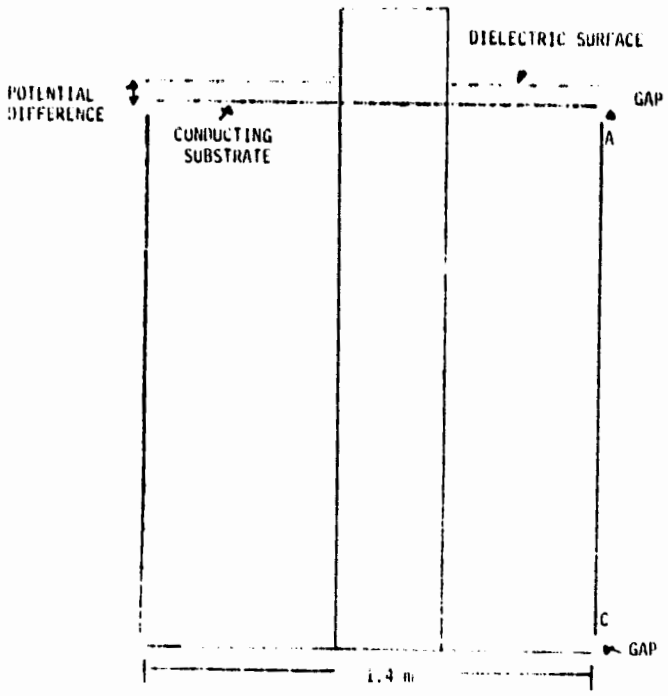

Figure 3. Cross section of computer simulation model.

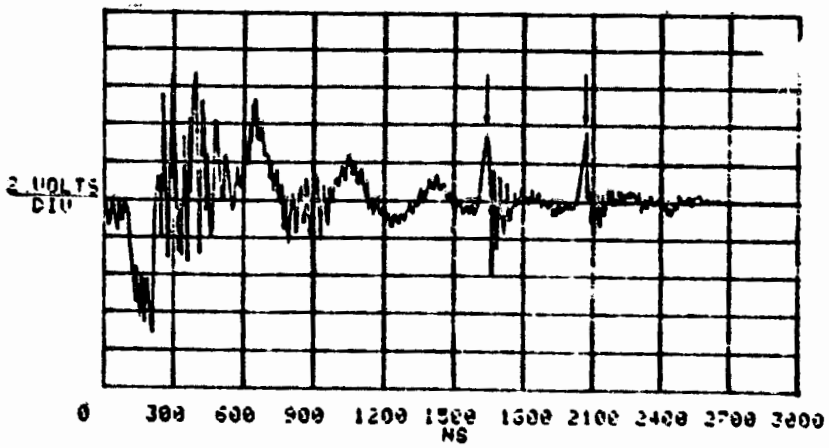

Figure 4. B time history showing multiple excitations (arrows).

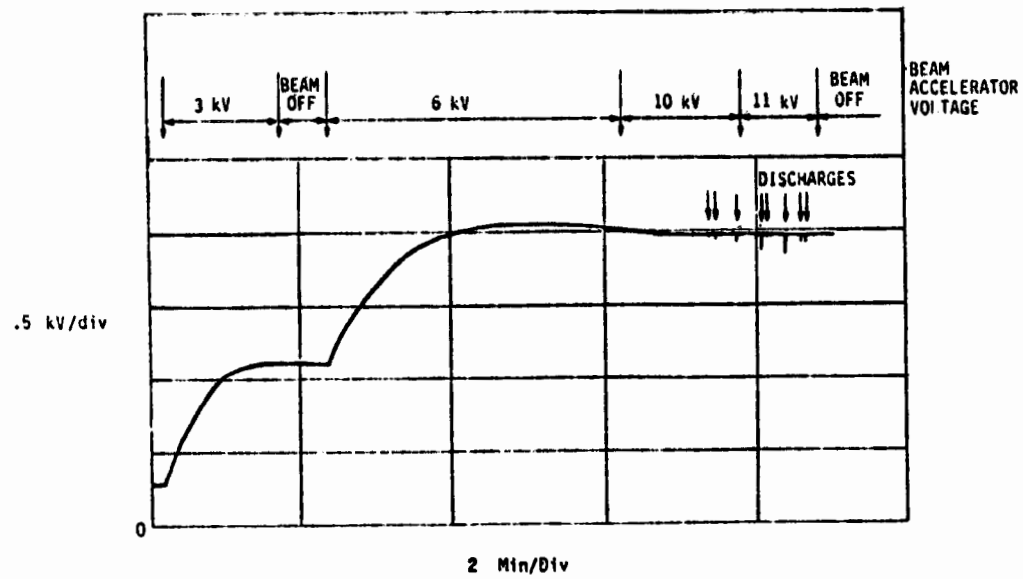

Figure 5. Electrostatic voltmeter trace of charging/discharging sequence of thermal blanket (charging rate 3×10^{-5} A/m^2).

Figure 6a. Typical E dot time history.

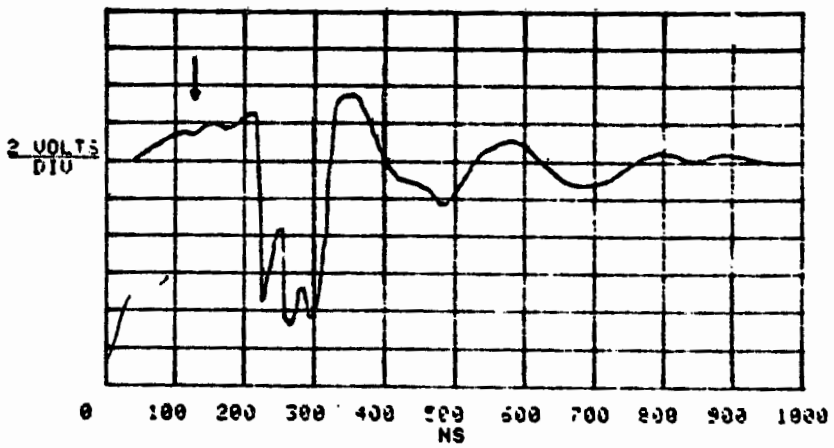

Figure 6b. Typical $\dot{E}$ time history.

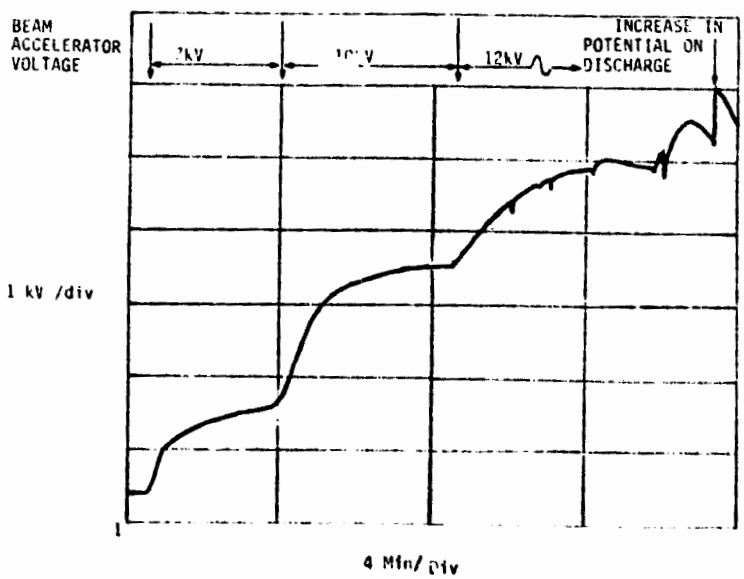

Figure 7a. Electrostatic voltmeter trace of solar cell charging time history (charging rate = 9×10^{-5} A/m^2).

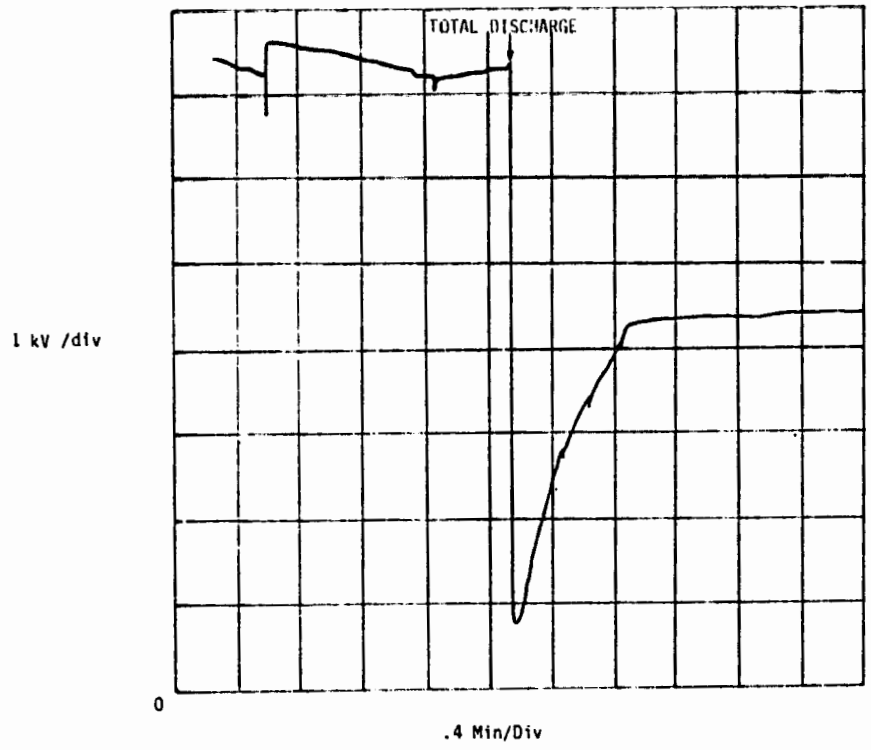

Figure 7b. Electrostatic voltmeter trace of solar cell charging time history (charging rate = 3×10^{-5} A/m^2).

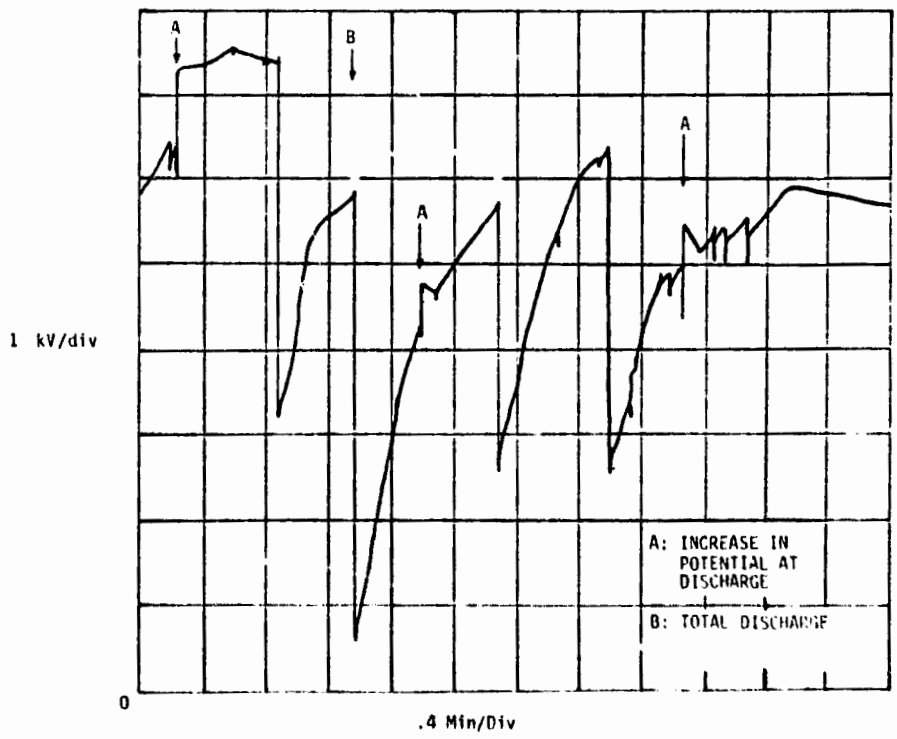

Figure 7c. Electrostatic voltmeter trace of solar cell charging time history (charging rate = 3×10^{-5} A/m^2).

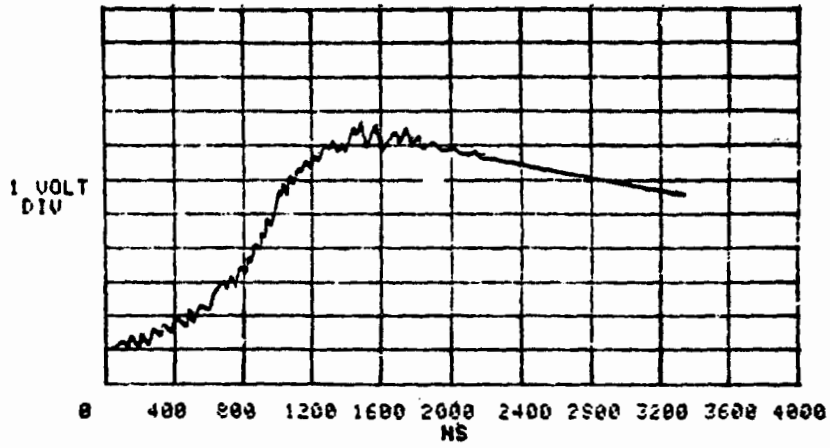

Figure 8a. Return current for solar cell illumination.

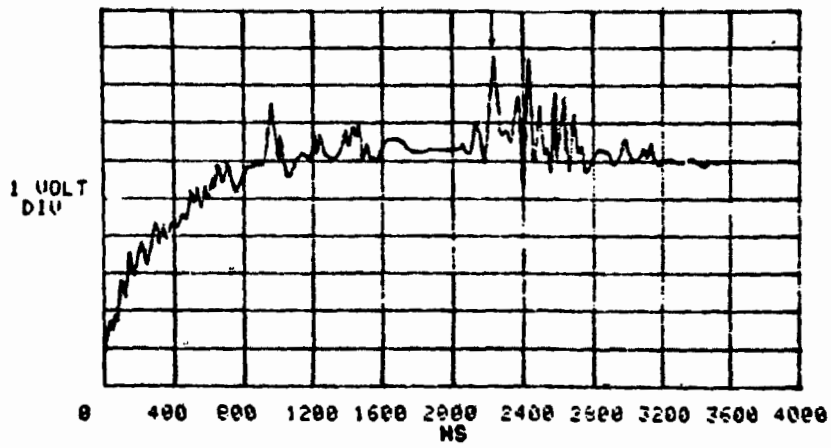

Figure 8b. Return current for solar cell illumination (arrow to second high frequency excitation).

·····Theoretical Predictions
—— Experimental Results

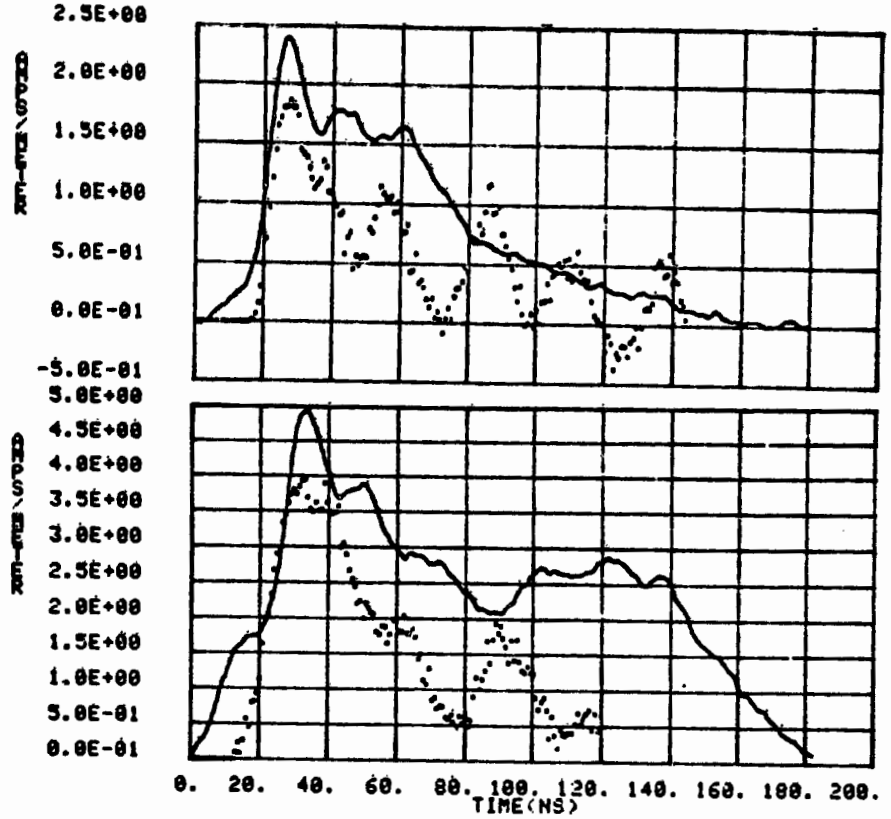

a) Without Precharging

b) With Precharging

Figure 9. External axial current density, thermal cover illumination.

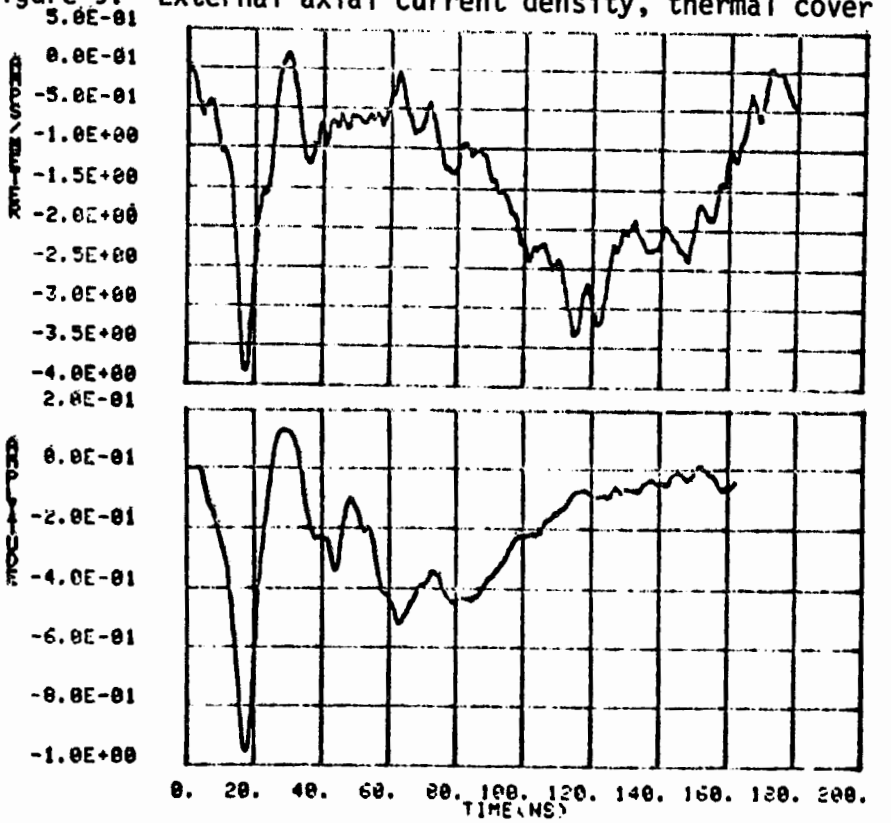

a) With Precharging

b) Without Precharging

Figure 10. External axial surface current density, solar panel illumination.

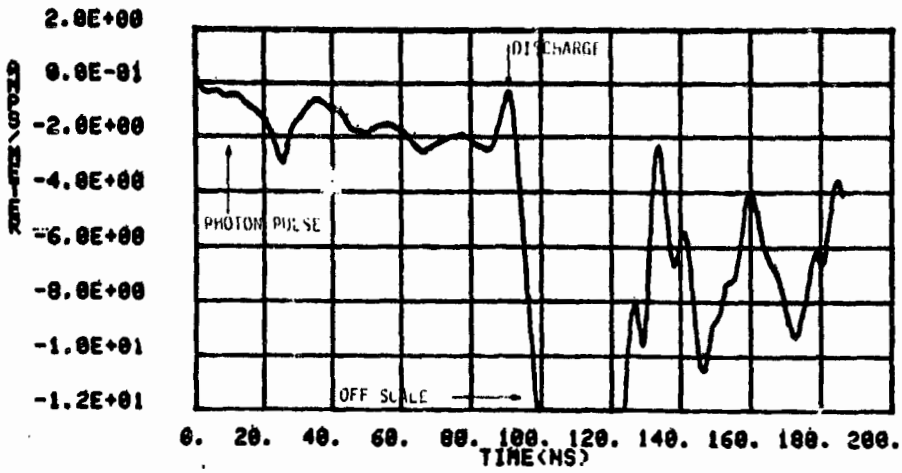

a) External Axial Surface Current Densit

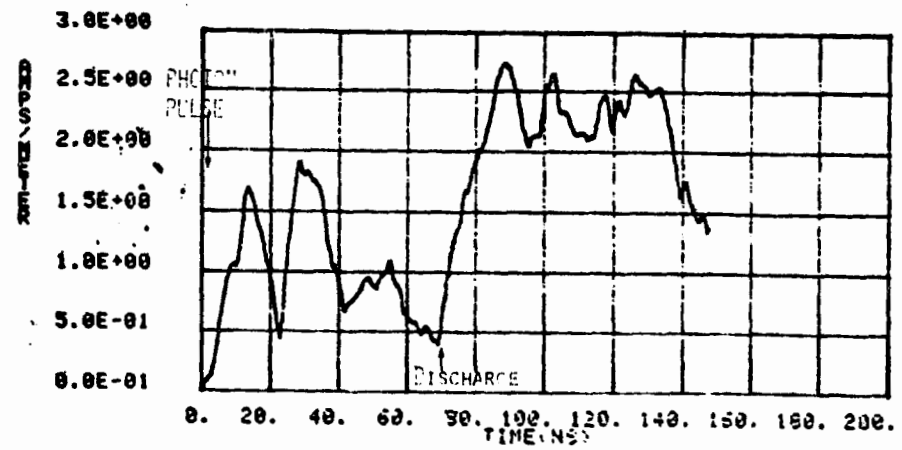

b) External Azimuthal Surface Current Density

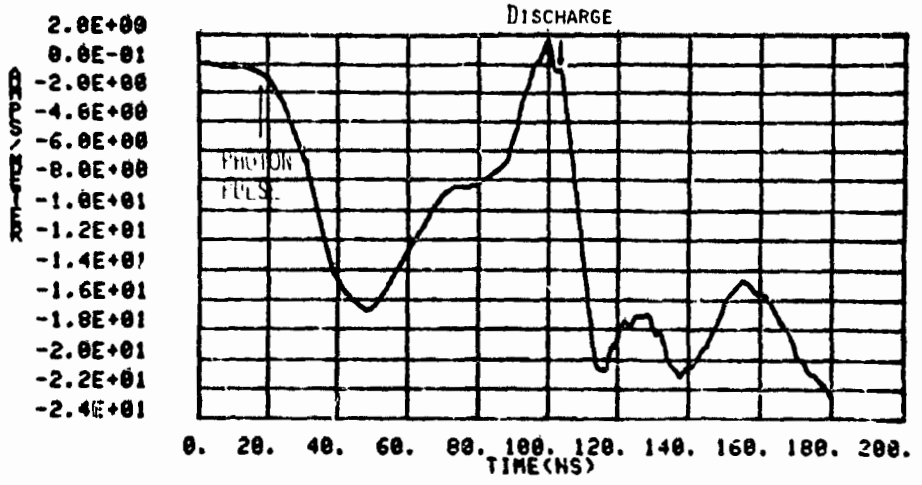

c) Surface Current Density Inside Solar Panel

Figure 11. Triggered Discharge

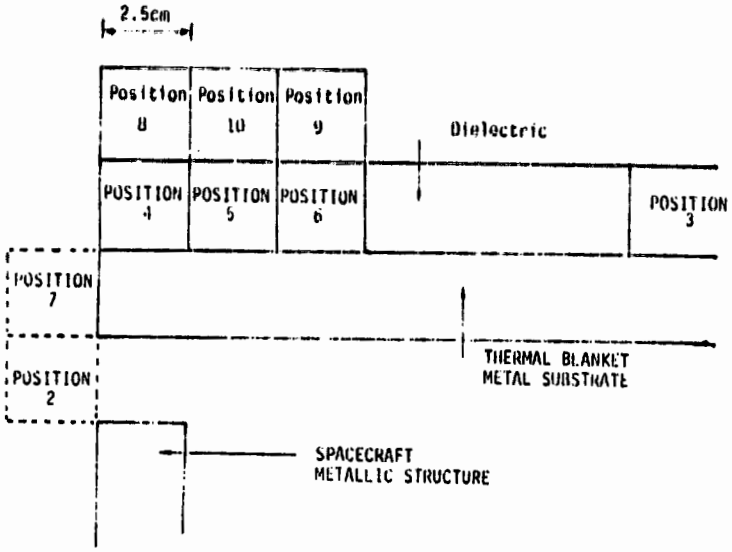

Figure 12a. Detail of computer model.

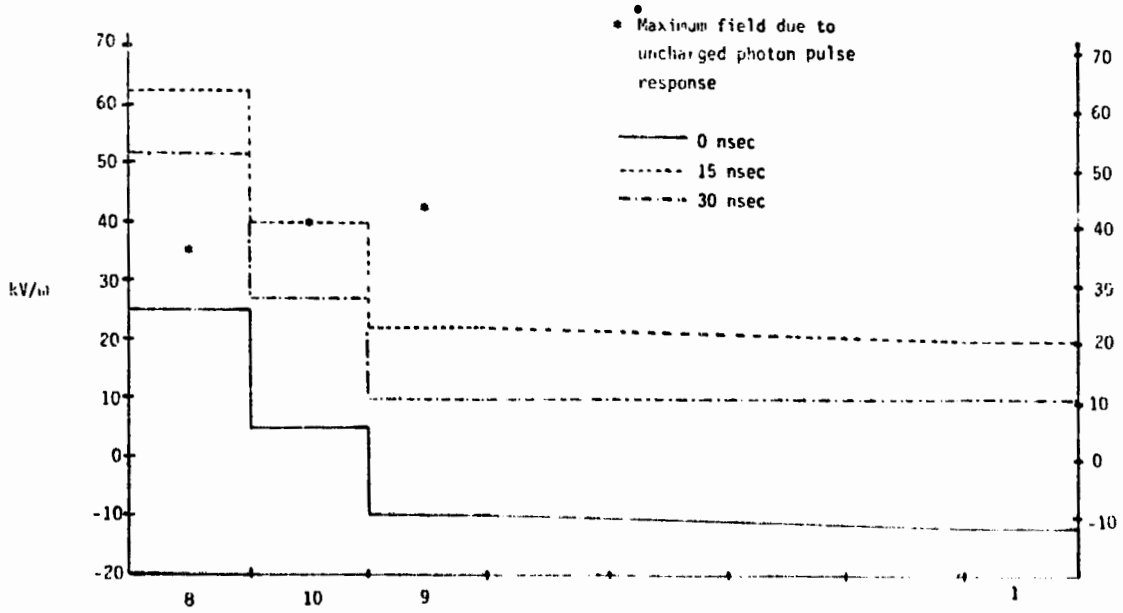

Figure 12b. Normal electric fields above the dielectric surface.